An Adaptive Artificial Viscosity Method for the Saint-Venant System

Yunlong Chen, Alexander Kurganov, Minlan Lei and Yu Liu

Abstract We develop an adaptive artificial viscosity method for the one-dimensional Saint-Venant system of shallow water equations. The proposed method is a semi-discrete finite-volume method based on an appropriate numerical flux and a high-order piecewise polynomial reconstruction. The latter is utilized without any computationally expensive nonlinear limiters, which are typically needed to guarantee nonlinear stability of the scheme. Instead, we enforce stability by adding an *adaptive artificial viscosity*, whose coefficients are proportional to the size of the weak local residual. Our method is capable to preserve the "lake at rest" steady state and the positivity of water depth. We test the proposed scheme on a number of benchmarks. The obtained numerical results clearly demonstrate that our method is well-balanced, positivity preserving and highly accurate.

1 Introduction

We are interested in applying the adaptive artificial viscosity method proposed in [13] to the Saint-Venant system of shallow water equations, which was first introduced in [25] and is still widely used to model flows in lakes, rivers, irrigation channels and coastal areas. In the one-dimensional case, the Saint-Venant system

Yunlong Chen
Mathematics Department, Tulane University, New Orleans, LA 70118, e-mail: ychen14@tulane.edu

Alexander Kurganov
Mathematics Department, Tulane University, New Orleans, LA 70118, e-mail: kurganov@math.tulane.edu; supported in part by the NSF Grant DMS-1115718

Minlan Lei
Mathematics Department, Tulane University, New Orleans, LA 70118, e-mail: mlei@tulane.edu

Yu Liu
Mathematics Department, Tulane University, New Orleans, LA 70118, e-mail: yliu3@tulane.edu

reads:

$$\begin{cases} h_t + q_x = 0, \\ q_t + \left(hu^2 + \frac{1}{2}gh^2\right)_x = -ghB_x, \end{cases} \tag{1}$$

where $h(x,t)$, $q(x,t)$ and $u(x,t) = q(x,t)/h(x,t)$ denote the water depth, discharge and velocity, respectively, $B(x)$ represents the bottom topography, and g is the gravity constant.

It is well-known that the systems (1) admits nonsmooth solutions that may contain shocks, rarefaction waves, and in the case of nonsmooth bottom topography, also contact discontinuities. Therefore, a good numerical method for (1) must be nonlinearly stable since linearly stable methods may develop large spurious oscillations and even blow up. Finite-volume Godunov-type schemes are popular tools for hyperbolic systems of balance laws and in particular for the Saint-Venant system (1). Godunov-type schemes form a class of projection-evolution methods, in which at each time step the computed solution is approximated by a global piecewise polynomial function (reconstructed from the captured discrete quantities, the cell averages), which is evolved in time to the next time level according to the integral form of the studied system of balance laws. The nonlinear stability of Godunov-type schemes is typically guaranteed by enforcing a non-oscillatory nature of the piecewise polynomial reconstruction with the help of nonlinear limiters. However, such limiters may be very complicated and computationally expensive. Alternatively, one may use less computationally expensive nonlimited reconstructions, while enforcing the nonlinear stability by adding an artificial viscosity to the PDE system in the regions where the computed solution is nonsmooth.

In this paper, we use a recently proposed adaptive artificial viscosity method, in which the viscosity coefficients are chosen to be proportional to the size of the weak local residual (WLR). The WLR is in turn proportional to Δ ($\Delta := \max(\Delta x, \Delta t)$, where Δx and Δt are small spatial and temporal scales, respectively) near (nonlinear) shocks, while it is much smaller ($\sim \Delta^\alpha$, α is close to 2) at (linear) contact waves and tiny in the smooth parts of the solution ($\sim \Delta^4$) (see [3, 9, 10, 13] for details). Therefore, the artificial viscosity vanishes as one refines the grid and the resulting adaptive artificial viscosity method is consistent. Moreover, the rate at which the viscosity coefficients decay, allows us to achieve the main goal—to stabilize the solution at shock regions without oversmearing contact discontinuities or affecting the high resolution of smooth parts of the computed solution. In order to make the adaptive artificial viscosity method robust, we tune the artificial viscosity coefficients following strategies in [6, 13]: The coefficients are first adjusted on a very coarse mesh and then used for the high-resolution computation on finer meshes.

It is well-known that a good numerical method for (1) should preserve positivity of computed values of h as well as to accurately capture steady states and their small perturbations (quasi-steady flows). The system (1) admits smooth steady-state solutions satisfying

$$hu \equiv \text{constant}, \quad \frac{u^2}{2} + g(h+B) \equiv \text{constant},$$

as well as nonsmooth steady-state solutions. Both are physically relevant and thus practically significant. One of the most important steady-state solutions is the following "lake at rest" steady state:

$$u \equiv 0, \quad h + B \equiv \text{constant.} \tag{2}$$

Schemes that are capable of exactly preserving such solutions are called well-balanced schemes. In the past decade, a number of well-balance and positivity preserving schemes has been introduced, see, e.g. [1, 2, 4, 7, 8, 11, 15, 18, 19, 20, 21, 22, 23, 24, 27, 28].

A good numerical scheme for (1) should also preserve the positivity of h. This is important since if h gets negative, numerical computation may break down because the eigenvalues of the flux Jacobian of (1) are $u \pm \sqrt{gh}$. In this paper, we develop an adaptive artificial viscosity method, which is guaranteed to be both positivity preserving and well-balanced by implementing the techniques from [15, 20].

This paper is organized as follows. In §2, we describe the adaptive artificial viscosity method for the Saint-Venant system (1). In §3, we apply the adaptive artificial viscosity method to a number of numerical examples. The obtained results indicate that our method is highly accurate, robust, well-balanced and positivity preserving.

2 Adaptive Artificial Viscosity Method

In this section, we describe the adaptive artificial viscosity method for the Saint-Venant system (1). For simplicity, we introduce a uniform spatial grid with the cells $I_j = (x_{j-\frac{1}{2}}, x_{j+\frac{1}{2}})$, where $x_\alpha = \alpha \Delta x$, $\forall \alpha$. We denote the vector of conservative variables by $\mathbf{U} := (h, q)^T$, the flux function by $\mathbf{f}(\mathbf{U}, B) := \left(q, hu^2 + \frac{1}{2}gh^2\right)^T$, the source term by $\mathbf{S}(\mathbf{U}, B) := (0, -ghB_x)^T$, and rewrite (1) in the following vector form:

$$\mathbf{U}_t + \mathbf{f}(\mathbf{U}, B)_x = \mathbf{S}(\mathbf{U}, B). \tag{3}$$

We then augment the system (3) with an adaptive artificial viscosity:

$$\mathbf{U}_t + \mathbf{f}(\mathbf{U}, B)_x = \mathbf{S}(\mathbf{U}, B) + C(\varepsilon(\mathbf{U})\mathbf{U}_x)_x, \tag{4}$$

where C is a tunable positive viscosity coefficient and $\varepsilon(\mathbf{U})$ is a nonnegative quantity, whose size is automatically adjusted depending on the local properties of $\mathbf{U}$. For computed solutions, we will make $\varepsilon(\mathbf{U})$ proportional to the WLR: This is one of the key points in our method, which will be obtained by discretizing (4) rather than (3).

The semi-discrete form of the adaptive artificial viscosity method reads

$$\frac{d}{dt}\overline{\mathbf{U}}_j = -\frac{\mathbf{H}_{j+\frac{1}{2}} - \mathbf{H}_{j-\frac{1}{2}}}{\Delta x} + \overline{\mathbf{S}}_j + C\left(\frac{\varepsilon_{j+\frac{1}{2}}\Delta\overline{\mathbf{U}}_{j+\frac{1}{2}} - \varepsilon_{j-\frac{1}{2}}\Delta\overline{\mathbf{U}}_{j-\frac{1}{2}}}{(\Delta x)^2}\right), \tag{5}$$

where

$$\overline{\mathbf{U}}_j := \frac{1}{\Delta x} \int\limits_{I_j} \mathbf{U}(x,t)\,dx$$

denotes the jth cell averages of the computed solution, $\mathbf{H}_{j\pm\frac{1}{2}}$ is a linearly stable numerical flux, and

$$\overline{\mathbf{S}}_j(t) = (0, \overline{S}_j^{(2)})^T, \quad \overline{S}_j^{(2)} \approx -\frac{g}{\Delta x} \int\limits_{I_j} h B_x\,dx \tag{6}$$

is an appropriate quadrature for the cell average of the geometric source term. The last term on the right hand side (RHS) of (5) is the adaptive artificial viscosity term, in which $\Delta \overline{\mathbf{U}}_{j+\frac{1}{2}} := \overline{\mathbf{U}}_{j+1} - \overline{\mathbf{U}}_j$ and $\varepsilon_{j+\frac{1}{2}} := \max(|E_{j-\frac{1}{2}}|, |E_{j+\frac{1}{2}}|, |E_{j+\frac{3}{2}}|)$, where $E_{j+\frac{1}{2}}$ is the WLR for the first equation in (1):

$$\begin{aligned}
E_{j+\frac{1}{2}} = \frac{\Delta x}{6} \Big[& h_{j+\frac{3}{2}}(t) - h_{j+\frac{3}{2}}(t-\Delta t) + 4\big(h_{j+\frac{1}{2}}(t) - h_{j+\frac{1}{2}}(t-\Delta t)\big) \\
& + h_{j-\frac{1}{2}}(t) - h_{j-\frac{1}{2}}(t-\Delta t) \Big] \\
& + \frac{\Delta t}{4} \Big[q_{j+\frac{3}{2}}(t) - q_{j-\frac{1}{2}}(t) + q_{j+\frac{3}{2}}(t-\Delta t) - q_{j-\frac{1}{2}}(t-\Delta t) \Big],
\end{aligned} \tag{7}$$

where all of the participating point values of h and q are obtained using a piecewise polynomial reconstruction discussed below. Observe that formula (7), which was derived in [13] (see also [3, 9, 10]), requires data from both the current and previous time level. Therefore, our adaptive artificial viscosity method can only be used starting from the second time step. In the first step, one has to use a high resolution scheme stabilized using a certain nonlinear limiter.

We stress that the proposed adaptive artificial viscosity method is not tied to any specific numerical flux. In our numerical experiments, we have used the central-upwind flux developed in [14] (see also [12, 16]):

$$\begin{aligned}
\mathbf{H}_{j+\frac{1}{2}} = & \frac{a_{j+\frac{1}{2}}^+ \mathbf{f}\big(\mathbf{U}_{j+\frac{1}{2}}^-, B_{j+\frac{1}{2}}\big) - a_{j+\frac{1}{2}}^- \mathbf{f}\big(\mathbf{U}_{j+\frac{1}{2}}^+, B_{j+\frac{1}{2}}\big)}{a_{j+\frac{1}{2}}^+ - a_{j+\frac{1}{2}}^-} \\
& + \frac{a_{j+\frac{1}{2}}^+ a_{j+\frac{1}{2}}^-}{a_{j+\frac{1}{2}}^+ - a_{j+\frac{1}{2}}^-} \Big[\mathbf{U}_{j+\frac{1}{2}}^+ - \mathbf{U}_{j+\frac{1}{2}}^- \Big].
\end{aligned} \tag{8}$$

where $a_{j+\frac{1}{2}}^\pm$ are the local one-sided speeds defined in (19) below, and $\mathbf{U}_{j+\frac{1}{2}}^\pm = (h_{j+\frac{1}{2}}^\pm, q_{j+\frac{1}{2}}^\pm)^T$ are the right/left point values of the conservative variables h and q at the cell interface $x = x_{j+\frac{1}{2}}$ obtained using a nonlimited conservative fifth-order piecewise polynomial reconstruction (see [13] for details). We note that in order to obtain a well-balanced scheme, one needs to reconstruct the equilibrium variables $w := h + B$ and q rather than the conservative ones. This results in

$$w^+_{j+\frac{1}{2}} = \frac{1}{60}\left(-3\overline{w}_{j-1} + 27\overline{w}_j + 47\overline{w}_{j+1} - 13\overline{w}_{j+2} + 2\overline{w}_{j+3}\right),$$

$$w^-_{j+\frac{1}{2}} = \frac{1}{60}\left(2\overline{w}_{j-2} - 13\overline{w}_{j-1} + 47\overline{w}_j + 27\overline{w}_{j+1} - 3\overline{w}_{j+2}\right),$$

$$q^+_{j+\frac{1}{2}} = \frac{1}{60}\left(-3\overline{q}_{j-1} + 27\overline{q}_j + 47\overline{q}_{j+1} - 13\overline{q}_{j+2} + 2\overline{q}_{j+3}\right), \qquad (9)$$

$$q^-_{j+\frac{1}{2}} = \frac{1}{60}\left(2\overline{q}_{j-2} - 13\overline{q}_{j-1} + 47\overline{q}_j + 27\overline{q}_{j+1} - 3\overline{q}_{j+2}\right),$$

and the corresponding point values of h are obtained using

$$h^{\pm}_{j+\frac{1}{2}} = w^{\pm}_{j+\frac{1}{2}} - B_{j+\frac{1}{2}}. \qquad (10)$$

Here,

$$B_{j+\frac{1}{2}} := \frac{B(x_{j+\frac{1}{2}} + 0) + B(x_{j+\frac{1}{2}} - 0)}{2},$$

which reduces to $B_{j+\frac{1}{2}} = B(x_{j+\frac{1}{2}})$ if the bottom topography is continuous.

Remark 1. The system of ODEs (5) should be solved using a stable and sufficiently accurate ODE solver. In all of our numerical examples, we have used the third-order strong stability preserving (SSP) Runge-Kutta method from [5].

Remark 2. We note that all of the terms (except for B) in (5), (6), (8)–(10) depend on time, but this dependence is suppressed for notational convenience.

Remark 3. In the evaluation of the WLR in (7), one has to use point values of h and q at the cell interfaces. Our reconstruction (9), (10) provides us with two point values of each of the variables at every cell interface. One can use any of these values in (7). In our numerical experiments, we have used the left values, that is, we have taken $h_{j+\frac{1}{2}} = h^-_{j+\frac{1}{2}}$ and $q_{j+\frac{1}{2}} = q^-_{j+\frac{1}{2}}$ for all j at both the current and previous time levels.

Remark 4. To ensure positivity of h, we follow [15] and replace the bottom topography function B with its continuous piecewise linear approximation

$$\widetilde{B}(x) = B_{j-\frac{1}{2}} + \left(B_{j+\frac{1}{2}} - B_{j-\frac{1}{2}}\right) \cdot \frac{x - x_{j-\frac{1}{2}}}{\Delta x}, \quad x_{j-\frac{1}{2}} \le x \le x_{j+\frac{1}{2}}, \qquad (11)$$

so that we set

$$B_j := \widetilde{B}(x_j) = \frac{1}{\Delta x}\int_{I_j}\widetilde{B}(x)\,dx = \frac{B_{j+\frac{1}{2}} + B_{j-\frac{1}{2}}}{2}.$$

Notice that this affects the numerical solution and its accuracy in dry ($h = 0$) and almost dry ($h \sim 0$) areas only, where the studied Saint-Venant system is not so accurate to begin with. Replacing B with $\widetilde{B}$ also reduces the formal order of the source term quadrature, which will be described in §2.1 below.

2.1 Source Term Quadrature

The construction of a well-balanced scheme hinges on the use of a special well-balanced quadrature for the source term $\overline{\mathbf{S}}_j$ in (6). We use the fourth-order Simpson-type well-balanced quadrature proposed in [20]. In the case of the piecewise linear bottom topography $\widetilde{B}$ (11), this quadrature reduces to

$$\overline{S}_j^{(2)} \approx -\frac{g}{6}\left(h_{j+\frac{1}{2}}^- + 4h_j + h_{j-\frac{1}{2}}^+\right)\frac{B_{j+\frac{1}{2}} - B_{j-\frac{1}{2}}}{\Delta x}. \qquad (12)$$

Here, h_j is the point value of h at the jth cell center obtained using the same non-limited conservative fifth-order piecewise polynomial reconstruction for w, which was used in (9) to obtain the endpoint values in the jth cell:

$$h_j = \frac{1}{1920}\left(9\overline{w}_{j-2} - 116\overline{w}_{j-1} + 2134\overline{w}_j - 116\overline{w}_{j+1} + 9\overline{w}_{j+2}\right) - B_j. \qquad (13)$$

We would like to point out that the artificial viscosity term $C(\varepsilon(\mathbf{U})\mathbf{U}_x)_x$ in the second equation of (4) does not affect the well-balanced property of the scheme because $q \equiv 0$ in the "lake at rest" stead state.

2.2 Correction of the Reconstructed Point Values

Recall that the designed scheme should preserve the positivity of the water depth h. Notice that the positivity of $h_{j+\frac{1}{2}}^\pm$, obtained in (10), is not guaranteed unless $w_{j+\frac{1}{2}}^\pm \geq B_{j+\frac{1}{2}}$. Therefore, the reconstructed point values $w_{j+\frac{1}{2}}^\pm$ may need to be corrected. To do so, we first consider the quantity

$$\widehat{h}_j := \overline{h}_j - \frac{1}{3}\left(h_{j+\frac{1}{2}}^- + h_{j-\frac{1}{2}}^+\right), \qquad (14)$$

and notice that if the solution is smooth and cell j is not (almost) dry, then $\widehat{h}_j \geq 0$. Indeed, using the Taylor expansion, one may obtain that for the exact smooth solution formula (14) gives

$$\widehat{h}_j = \frac{1}{\Delta x}\int_{I_j} h(x,t)\,dx - \frac{1}{3}\left(h(x_{j+\frac{1}{2}},t) + h(x_{j-\frac{1}{2}},t)\right)$$

$$= \frac{1}{3}h(x_j,t) - \frac{1}{24}(\Delta x)^2 h_{xx}(x_j,t) + \mathcal{O}\left((\Delta x)^4\right),$$

which is nonnegative provided $h(x_j,t)$ is not too small and $h_{xx}(x_j,t)$ is not too large. If $\widehat{h}_j < 0$ at some cell j, then the positivity proof in §2.4 would fail and to ensure positivity we replace the nonlimited fifth-order reconstruction of w with the nonlimited

second-order Fromm's reconstruction (see, e.g., [18]) which gives

$$w^+_{j+\frac{1}{2}} = \frac{1}{4}\left(\overline{w}_j + 4\overline{w}_{j+1} - \overline{w}_{j+2}\right), \quad w^-_{j+\frac{1}{2}} = \frac{1}{4}\left(-\overline{w}_{j-1} + 4\overline{w}_j + \overline{w}_{j+1}\right). \quad (15)$$

For the piecewise linear reconstruction, $\widehat{h}_j = \overline{h}_j/6$, and it is obviously positive provided $\overline{h}_j > 0$. However, the values of $h^\pm_{j+\frac{1}{2}}$ calculated from either (9) or (15) may be negative. If this occurs, we follow the approach from [15] and make another correction: We replace the jth piece of the reconstruction with a linear piece, which is adjusted to the corresponding linear piece of $\widetilde{B}$ and has the following endpoint values:

$$\begin{aligned}
&\text{if } w^-_{j+\frac{1}{2}} < B_{j+\frac{1}{2}}, \quad \text{then take } w^-_{j+\frac{1}{2}} = B_{j+\frac{1}{2}}, \ \ w^+_{j-\frac{1}{2}} = 2\overline{w}_j - B_{j+\frac{1}{2}}; \\
&\text{if } w^+_{j-\frac{1}{2}} < B_{j-\frac{1}{2}}, \quad \text{then take } w^-_{j+\frac{1}{2}} = 2\overline{w}_j - B_{j-\frac{1}{2}}, \ \ w^+_{j-\frac{1}{2}} = B_{j-\frac{1}{2}}.
\end{aligned} \quad (16)$$

This correction procedure guarantees that the resulting reconstruction of w will remain conservative and will stay above the piecewise linear approximant of the bottom topography $\widetilde{B}$. Therefore, the point values $h^\pm_{j+\frac{1}{2}}$, computed from (10), will be nonnegative.

2.3 Desingularization

Even though both the cell averages $\overline{h}_j$ and point values $h^\pm_{j+\frac{1}{2}}$ are nonnegative, they may be very small or even zero, which may be troublesome in calculating the velocities $u^\pm_{j+\frac{1}{2}}$. To overcome this difficulty, we follow [15] and desingularize the division $u^\pm_{j+\frac{1}{2}} = q^\pm_{j+\frac{1}{2}}/h^\pm_{j+\frac{1}{2}}$ by replacing it with

$$u^\pm_{j+\frac{1}{2}} = \frac{\sqrt{2}\,h^\pm_{j+\frac{1}{2}}q^\pm_{j+\frac{1}{2}}}{\sqrt{(h^\pm_{j+\frac{1}{2}})^4 + \max((h^\pm_{j+\frac{1}{2}})^4, \delta)}}, \quad (17)$$

where δ is a small positive number chosen in our numerical experiments to be between $(\Delta x)^4$ and $(\Delta x)^2$. For consistency of the resulting scheme, we then use the recalculated values of $u^\pm_{j+\frac{1}{2}}$ to recompute the discharges q at the cell interfaces:

$$q^\pm_{j+\frac{1}{2}} := h^\pm_{j+\frac{1}{2}} \cdot u^\pm_{j+\frac{1}{2}}. \quad (18)$$

Equipped with the point values of both $h^\pm_{j+\frac{1}{2}}$ and $u^\pm_{j+\frac{1}{2}}$, we can now calculate the one-sided local speeds of propagation, which are obtained using the eigenvalues of the Jacobian as follows:

$$a^+_{j+\frac{1}{2}} = \max \left\{ u^+_{j+\frac{1}{2}} + \sqrt{gh^+_{j+\frac{1}{2}}}, u^-_{j+\frac{1}{2}} + \sqrt{gh^-_{j+\frac{1}{2}}}, 0 \right\},$$

$$a^-_{j+\frac{1}{2}} = \min \left\{ u^+_{j+\frac{1}{2}} - \sqrt{gh^+_{j+\frac{1}{2}}}, u^-_{j+\frac{1}{2}} - \sqrt{gh^-_{j+\frac{1}{2}}}, 0 \right\}. \tag{19}$$

2.4 Positivity Preserving Property

In this section, we prove the positivity preserving property of the proposed adaptive artificial viscosity method. Notice that the technique used to prove the positivity of the central-upwind scheme in [11, 15] cannot be directly applied to our method since for a nonlimited conservative fifth-order piecewise polynomial reconstruction

$$\overline{h}_j \neq \frac{h^-_{j+\frac{1}{2}} + h^+_{j-\frac{1}{2}}}{2}.$$

However, the correction procedure described in §2.2 allows one to easily prove the main result of this section.

Theorem 1. *Consider the system (4) and the adaptive artificial viscosity method (5)–(18). Assume that the system of ODEs (5) is solved by the forward Euler method, and that the solution at time level $t = t^n$ satisfies $\overline{h}^n_j \geq 0$ for all j. Then at the next time level $\overline{h}^{n+1}_j \geq 0$ for all j, provided that*

$$\Delta t \leq \frac{\Delta x}{4} \min \left\{ \frac{1}{a}, \frac{\Delta x}{C \max_j [\varepsilon_{j+\frac{1}{2}} + \varepsilon_{j-\frac{1}{2}}]} \right\}, \tag{20}$$

where $a := \max_j \left\{ \max\{a^+_{j+\frac{1}{2}}, -a^-_{j+\frac{1}{2}}\} \right\}$.

Proof. First, we apply the forward Euler method to (5) and obtain

$$\overline{h}^{n+1}_j = \overline{h}^n_j - \lambda \left[H^{(1)}_{j+\frac{1}{2}} - H^{(1)}_{j-\frac{1}{2}} \right] + \frac{C\lambda}{\Delta x} \left[\varepsilon_{j+\frac{1}{2}} (\overline{h}^n_{j+1} - \overline{h}^n_j) - \varepsilon_{j-\frac{1}{2}} (\overline{h}^n_j - \overline{h}^n_{j-1}) \right], \tag{21}$$

where $\lambda := \Delta t / \Delta x$. We now use (14) to obtain

$$\overline{h}^n_j = \frac{1}{4} \overline{h}^n_j + \frac{3}{4} \overline{h}^n_j = \frac{1}{4} \overline{h}^n_j + \frac{1}{4} \left(h^-_{j+\frac{1}{2}} + h^+_{j-\frac{1}{2}} \right) + \frac{3}{4} \widehat{h}^n_j. \tag{22}$$

Substituting the first component of (8), (18) and (22) into (21) results in

$$\overline{h}_j^{n+1} = \frac{3}{4}\widehat{h}_j^n + \left[\frac{1}{4} + \lambda a_{j-\frac{1}{2}}^- \left(\frac{a_{j-\frac{1}{2}}^+ - u_{j-\frac{1}{2}}^+}{a_{j-\frac{1}{2}}^+ - a_{j-\frac{1}{2}}^-}\right)\right] h_{j-\frac{1}{2}}^+$$

$$+ \left[\frac{1}{4} - \lambda a_{j+\frac{1}{2}}^+ \left(\frac{u_{j+\frac{1}{2}}^- - a_{j+\frac{1}{2}}^-}{a_{j+\frac{1}{2}}^+ - a_{j+\frac{1}{2}}^-}\right)\right] h_{j+\frac{1}{2}}^-$$

$$+ \lambda a_{j-\frac{1}{2}}^+ \left(\frac{u_{j-\frac{1}{2}}^- - a_{j-\frac{1}{2}}^-}{a_{j-\frac{1}{2}}^+ - a_{j-\frac{1}{2}}^-}\right) h_{j-\frac{1}{2}}^- - \lambda a_{j+\frac{1}{2}}^- \left(\frac{a_{j+\frac{1}{2}}^+ - u_{j+\frac{1}{2}}^+}{a_{j+\frac{1}{2}}^+ - a_{j+\frac{1}{2}}^-}\right) h_{j+\frac{1}{2}}^+ \tag{23}$$

$$+ \frac{C\lambda}{\Delta x}\left(\varepsilon_{j+\frac{1}{2}}\overline{h}_{j+1}^n + \varepsilon_{j-\frac{1}{2}}\overline{h}_{j-1}^n\right) + \left[\frac{1}{4} - \frac{C\lambda}{\Delta x}\left(\varepsilon_{j+\frac{1}{2}} + \varepsilon_{j-\frac{1}{2}}\right)\right]\overline{h}_j^n.$$

Next, we argue as in [15] claiming that provided the CFL condition (20) is satisfied, $\overline{h}_j^{n+1}$ in (23) is a linear combination of nonnegative quantities ($\widehat{h}_j^n$, $h_{j\pm\frac{1}{2}}^\pm$, $\overline{h}_{j\pm1}^n$ and $\overline{h}_j^n$) with nonnegative coefficients. This completes the proof of the theorem. □

Remark 5. Notice that since the maximal value of $\varepsilon_{j+\frac{1}{2}}$ is at most proportional to Δx, the time step restriction (20) is not severe since Δt is still proportional to Δx and not to $(\Delta x)^2$.

Remark 6. The positivity proof can be directly extended from the forward Euler to the SSP ODE solvers from [5].

3 Numerical Examples

In this section, we demonstrate the performance of our adaptive artificial viscosity (AAV) method on a number of test problems. All of the reference solutions are computed using the second-order central-upwind scheme with the piecewise linear minmod reconstruction ([15]) on a much finer mesh with $\Delta x = 1/6400$.

Example 1 – Small Perturbation of a Steady-State Solution

In this example taken from LeVeque [17], we numerically solve the Saint-Venant system (1) with $g = 1$ and the non-flat bottom topography containing one hump:

$$B(x) = \begin{cases} 0.25\left(\cos(10\pi(x-0.5)) + 1\right), & 0.4 \le x \le 0.6, \\ 0, & \text{otherwise.} \end{cases} \tag{24}$$

The initial data is the perturbed stationary solution:

$$w(x,0) = 1 + \sigma, \quad u(x,0) = 0,$$

where the perturbation constant σ is non-zero on the interval $[0.1, 0.2]$. We compare the performance of the AAV method with different viscosity coefficient C. The obtained solutions are presented in Figures 1 and 2, respectively. The AAV constants are taken as $C = 10$ and $C = 70$. The obtained results are of a comparable quality: The achieved resolution is quite sharp and the AAV method is not too sensitive to the selection of the AAV constant C for both large ($\sigma = 10^{-2}$) and small ($\sigma = 10^{-5}$) perturbations.
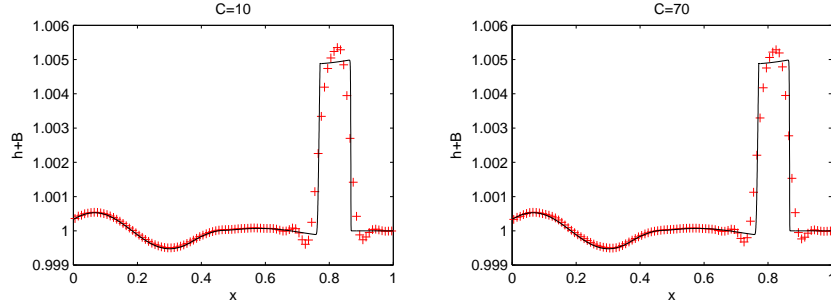
Fig. 1: Example 1. $\sigma = 10^{-2}$, water surface $h + B$ at time $t = 0.7$ computed by the AAV method using the uniform mesh with $\Delta x = 1/100$. The solid line is the reference solution.
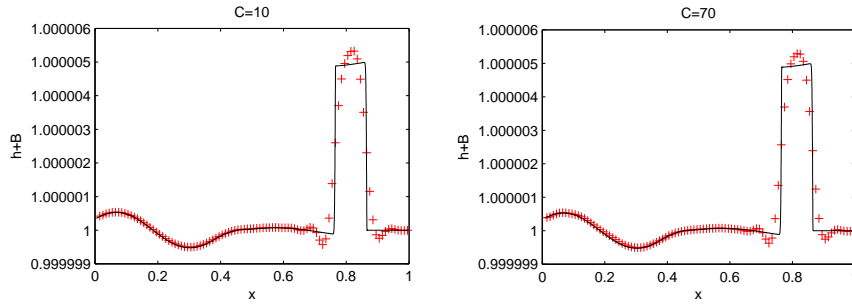
Fig. 2: Example 1. The same as Figure 1 but with $\sigma = 10^{-5}$.

Example 2 – Transcritical Flow

This example is also taken from [17]. We numerically solve the Saint-Venant system with $g = 1$, the same bottom topography function (24) and the following initial data:

$$w = 1, \quad u = 0.3.$$

In this example, the flow is transcritical, which means the Froude number $Fr = u/\sqrt{gh}$ can pass through 1 and thus one of the eigenvalues $u \pm \sqrt{gh}$ passes through 0. In such case, the steady-state solution contains a stationary shock. The numerical solution computed by the AAV method with $C = 20$ is presented in Figure 3. As one can clearly see, the stationary shock is very well resolved.
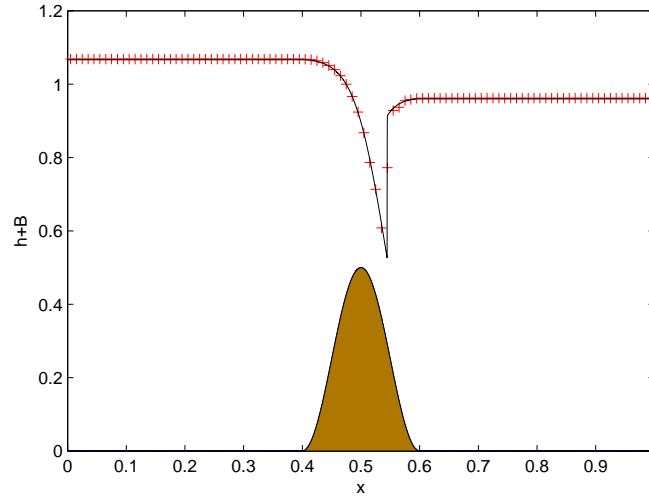

Fig. 3: Example 2. Water surface $h + B$ at time $t = 1.8$ computed by the AAV method using the uniform mesh with $\Delta x = 1/100$. The solid line is the reference solution.

Example 3 – Dam-Break Problem over the Flat Bottom

In this example, we consider the dam-break problem for the Saint-Venant system with $g = 1$ over a flat bottom ($B \equiv 0$) and subject to the following Riemann initial data:

$$(h, u)^T (x, 0) = \begin{cases} (3, 0)^T, & x < 0, \\ (1, 0)^T, & x > 0. \end{cases}$$

The solution consisting of a rarefaction wave and a shock wave is computed by the AAV method with $C = 8$. The obtained water depth h is presented in Figure 4. As one can clearly see, both waves are sharply and accurately resolved by the AAV method.
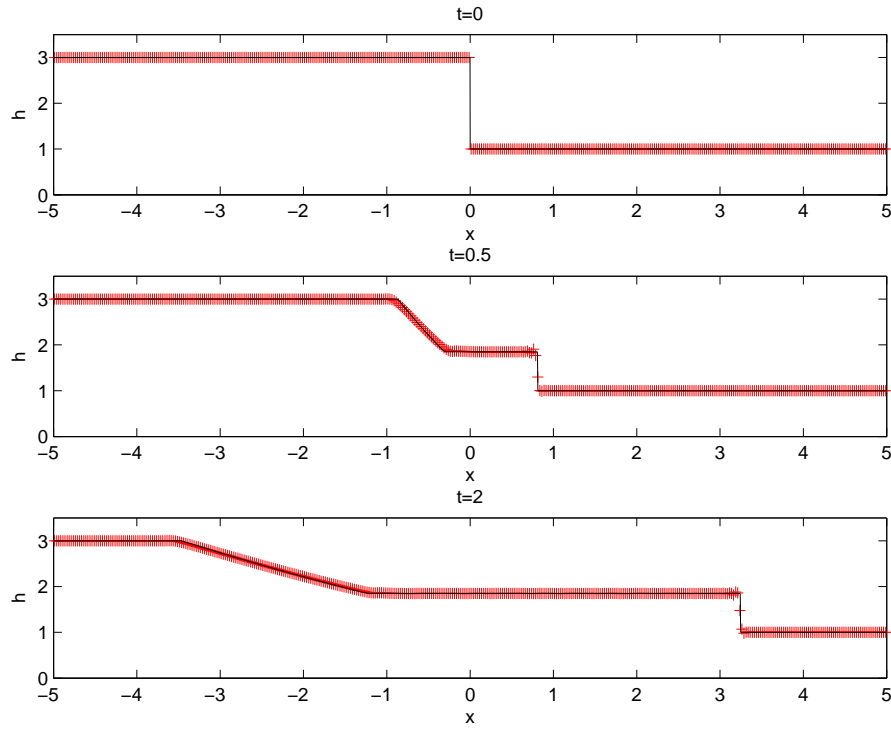
Fig. 4: Example 3. Water depth h at times $t = 0.5$ and $t = 2$ computed by the AAV method using the uniform mesh with $\Delta x = 0.025$. The solid line is the reference solution.

Example 4 – Dam-Break Problem over a Rectangular Bump

In this example taken from [26], we numerically solve the dam-break problem for the Saint-Venant system with $g = 9.812$ over a rectangular bump. The bottom topography is the following discontinuous function:

$$B(x) = \begin{cases} 8, & \text{if } |x - 750| \le 187.5, \\ 0, & \text{otherwise}, \end{cases}$$

and the initial data are

$$(w, u)^T(x, 0) = \begin{cases} (20, 0)^T, & x < 750, \\ (15, 0)^T, & x > 750. \end{cases}$$

The water depth h is initially discontinuous at $x = 562.5$ and $x = 937.5$, which are the two locations of the discontinuous bottom edges. At time $t \approx 17$, the waves

reach those two edges and after this, the system generates several waves including transmitted, reflected and standing waves.

In Figure 5, we show the solution computed by the AAV method with $C = 10$ at small time ($t = 15$), that is, before any wave interactions. The solution shown in Figure 6 is at large time ($t = 55$), that is, after several wave interactions. At both times, the achieved resolution is very high and the obtained solution is almost non-oscillatory.
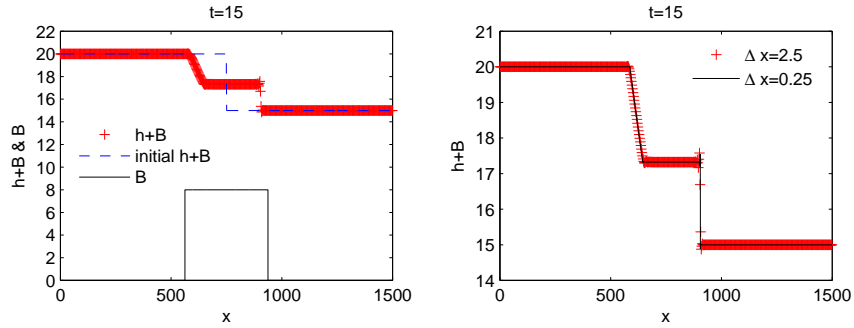

Fig. 5: Example 4. Water surface $h + B$ at small time ($t = 15$) computed by the AAV method using the uniform mesh. Left: $\Delta x = 2.5$, the water surface is plotted together with the initial condition and the bottom topography; Right: $\Delta x = 2.5$ and $\Delta x = 0.25$.
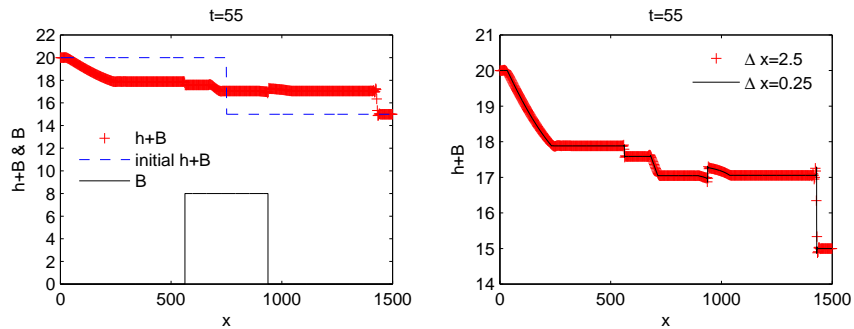

Fig. 6: Example 4. The same as Figure 5 but at large time ($t = 55$).

Example 5 – Saint-Venant System with Friction and Discontinuous Bottom

In this example taken from [15], we numerically solve the Saint-Venant system with an additional friction term $-\kappa(h)u$ on the RHS. The system then takes the form

$$\begin{cases} h_t + (hu)_x = 0, \\ (hu)_t + \left(hu^2 + \frac{1}{2}gh^2\right)_x = -ghB' - \kappa(h)u. \end{cases} \tag{25}$$

We take $g = 1$, the friction coefficient $\kappa(h) = 0.001(1 + 10h)^{-1}$, and the bottom topography

$$B(x) = \begin{cases} 1, & x < 0, \\ \cos^2(\pi x), & 0 \leq x \leq 0.4, \\ \cos^2(\pi x) + 0.25(\cos(10\pi(x - 0.5)) + 1), & 0.4 \leq x \leq 0.5, \\ 0.5\cos^4(\pi x) + 0.25(\cos(10\pi(x - 0.5)) + 1), & 0.5 \leq x \leq 0.6, \\ 0.5\cos^4(\pi x), & 0.6 \leq x \leq 1, \\ 0.25\sin^2(2\pi(x - 1)) & 1 < x \leq 1.5, \\ 0, & x > 1.5, \end{cases}$$

which has a discontinuity at $x = 1$. The initial data are

$$(h, u)^T(x, 0) = \begin{cases} (1.4 - B(x), 0)^T, & -0.25 < x < 0, \\ (0, 0), & 0 < x < 1.75. \end{cases}$$

This setting corresponds to the situation when the second of the three dams, initially located at $x = -0.25$, 0 and 1.75, breaks down at time $t = 0$, the water propagates into the initially dry area $[0, 1.75]$, and a stationary steady state is achieved after a certain time. We apply the AAV method to this problem. The cell average of the frictional term in (25) is discretized using Simpson's rule as follows:

$$\frac{1}{\Delta x} \int_{I_j} \frac{0.001\, u}{1 + 10h} \, dx = 0.001 \left[\frac{1}{6} \cdot \frac{u_{j-\frac{1}{2}}^+}{1 + 10h_{j-\frac{1}{2}}^+} + \frac{2}{3} \cdot \frac{u_j}{1 + 10h_j} + \frac{1}{6} \cdot \frac{u_{j+\frac{1}{2}}^-}{1 + 10h_{j+\frac{1}{2}}^-} \right].$$

Here, u_j is the point value at the jth cell center, which can be calculated using the desingularization similar to (17):

$$u_j = \frac{\sqrt{2}\, h_j q_j}{\sqrt{(h_j)^4 + \max((h_j)^4, (\Delta x)^2)}}, \tag{26}$$

where the point value h_j is given by (13) and q_j is obtained in a similar way:

$$q_j = \frac{1}{1920} \left(9\overline{q}_{j-2} - 116\overline{q}_{j-1} + 2134\overline{q}_j - 116\overline{q}_{j+1} + 9\overline{q}_{j+2}\right).$$

Notice that this friction term affects neither the well-balanced (since $u \equiv 0$ at the "lake at rest" steady state) nor the positivity preserving (since the first equation has not been modified) properties of the proposed AAV method.

In Figures 7 and 8, we plot time snapshots of the solution computed by the AAV method with $C = 20$. One can clearly see the dynamics of the flow as the water moves from the region $[-0.25, 0]$ into the initially dry area $[0, 1.75]$ and gradually settles down to a stationary steady state. These results demonstrate that the proposed AAV method is both well-balanced and positivity preserving.
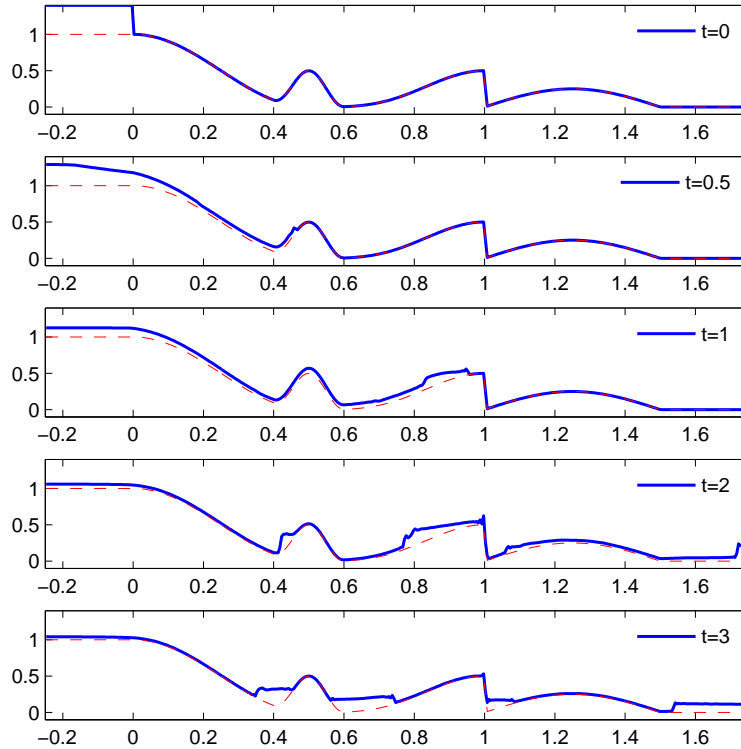

Fig. 7: Example 5. Water surface $h + B$ and bottom function B at times $t = 0$, 0.5, 1, 2 and 3 computed by the AAV method using the uniform mesh with $\Delta x = 1/100$.
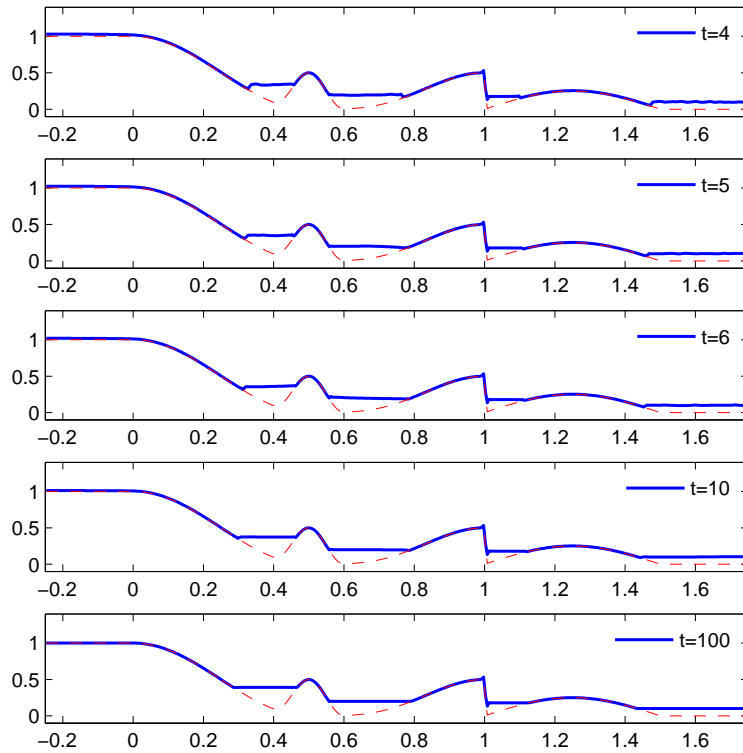
Fig. 8: Example 5. The same as Figure 7 but at times $t = 4$, 5, 6, 10 and 100. At time $t = 100$, when the stationary steady state is practically achieved, $\Delta x = 1/200$.

References

1. Audusse, E., Bouchut, F., Bristeau, M.O., Klein, R., Perthame, B.: A fast and stable well-balanced scheme with hydrostatic reconstruction for shallow water flows. SIAM J. Sci. Comput. **25**(6), 2050–2065 (electronic) (2004)
2. Bouchut, F.: Nonlinear stability of finite volume methods for hyperbolic conservation laws and well-balanced schemes for sources. Frontiers in Mathematics. Birkhäuser Verlag, Basel (2004)
3. Constantin, L.A., Kurganov, A.: Adaptive central-upwind schemes for hyperbolic systems of conservation laws. In: Hyperbolic problems: theory, numerics, applications (Osaka, 2004), pp. 95–103. Yokohama Publishers (2006)
4. Gallouët, T., Hérard, J.M., Seguin, N.: Some approximate Godunov schemes to compute shallow-water equations with topography. Comput. & Fluids **32**(4), 479–513 (2003)
5. Gottlieb, S., Shu, C.W., Tadmor, E.: Strong stability-preserving high-order time discretization methods. SIAM Rev. **43**(1), 89–112 (electronic) (2001)

6. Guermond, J.L., Pasquetti, R., Popov, B.: Entropy viscosity method for nonlinear conservation laws. J. Comput. Phys. **230**(11), 4248–4267 (2011)
7. Jin, S.: A steady-state capturing method for hyperbolic systems with geometrical source terms. M2AN Math. Model. Numer. Anal. **35**(4), 631–645 (2001)
8. Jin, S., Wen, X.: Two interface-type numerical methods for computing hyperbolic systems with geometrical source terms having concentrations. SIAM J. Sci. Comput. **26**(6), 2079–2101 (electronic) (2005)
9. Karni, S., Kurganov, A.: Local error analysis for approximate solutions of hyperbolic conservation laws. Adv. Comput. Math. **22**, 79–99 (2005)
10. Karni, S., Kurganov, A., Petrova, G.: A smoothness indicator for adaptive algorithms for hyperbolic systems. J. Comput. Phys. **178**, 323–341 (2002)
11. Kurganov, A., Levy, D.: Central-upwind schemes for the saint-venant system. M2AN Math. Model. Numer. Anal. **36**, 397–425 (2002)
12. Kurganov, A., Lin, C.T.: On the reduction of numerical dissipation in central-upwind schemes. Commun. Comput. Phys. **2**, 141–163 (2007)
13. Kurganov, A., Liu, Y.: New adaptive artificial viscosity method for hyperbolic systems of conservation laws. J. Comput. Phys. Submitted, available at `www.math.tulane.edu/~kurganov/Kurganov-Liu.pdf`
14. Kurganov, A., Noelle, S., Petrova, G.: Semi-discrete central-upwind scheme for hyperbolic conservation laws and Hamilton-Jacobi equations. SIAM J. Sci. Comput. **23**, 707–740 (2001)
15. Kurganov, A., Petrova, G.: A second-order well-balanced positivity preserving central-upwind scheme for the Saint-Venant system. Commun. Math. Sci **5**(1), 133–160 (2007)
16. Kurganov, A., Tadmor, E.: New high resolution central schemes for nonlinear conservation laws and convection-diffusion equations. J. Comput. Phys. **160**, 241–282 (2000)
17. LeVeque, R.J.: Balancing source terms and flux gradients in high-resolution Godunov methods: the quasi-steady wave-propagation algorithm. J. Comput. Phys. **146**(1), 346–365 (1998)
18. LeVeque, R.J.: Finite volume methods for hyperbolic problems. Cambridge Texts in Applied Mathematics. Cambridge University Press, Cambridge (2002)
19. Lukácová-Medvidová, M., Noelle, S., Kraft, M.: Well-balanced finite volume evolution Galerkin methods for the shallow water equations. J. Comput. Phys. **221**(1), 122–147 (2007)
20. Noelle, S., Pankratz, N., Puppo, G., Natvig, J.R.: Well-balanced finite volume schemes of arbitrary order of accuracy for shallow water flows. J. Comput. Phys. **213**(2), 474–499 (2006)
21. Noelle, S., Xing, Y., Shu, C.W.: High-order well-balanced finite volume WENO schemes for shallow water equation with moving water. J. Comput. Phys. **226**(1), 29–58 (2007)
22. Perthame, B., Simeoni, C.: A kinetic scheme for the Saint-Venant system with a source term. Calcolo **38**(4), 201–231 (2001)
23. Russo, G.: Central schemes for balance laws. In: Hyperbolic problems: theory, numerics, applications: proceedings of the Eighth International Conference in Magdeburg, February/March 2000, p. 821. Birkhauser (2002)
24. Russo, G.: Central schemes for conservation laws with application to shallow water equations. In: Trends and Applications of Mathematics to Mechanics, pp. 225–246. Springer Milan (2005)
25. de Saint-Venant, A.: Thèorie du mouvement non-permanent des eaux, avec application aux crues des rivière at à l'introduction des marèes dans leur lit. C.R. Acad. Sci. Paris **73**, 147–154 (1871)
26. Vukovic, S., Sopta, L.: ENO and WENO schemes with the exact conservation property for one-dimensional shallow water equations. J. Comput. Phys. **179**(2), 593–621 (2002)
27. Xing, Y., Shu, C.W.: High order finite difference WENO schemes with the exact conservation property for the shallow water equations. J. Comput. Phys. **208**(1), 206–227 (2005)
28. Xing, Y., Shu, C.W.: A new approach of high order well-balanced finite volume weno schemes and discontinuous galerkin methods for a class of hyperbolic systems with source terms. Commun. Comput. Phys. **1**, 100–134 (2006)